ANL/NDM--64

DE83 004437

ANL/NDM-64

THE FISSION-FRAGMENT ANGULAR DISTRIBUTIONS AND TOTAL KINETIC ENERGIES FOR $^{235}U(n,f)$ FROM .18 to 8.83 MeV[a]

by

J. W. Meadows and Carl Budtz-Jørgensen[b]

January 1982

[a]This work supported by the U.S. Department of Energy.

[b]Visiting scientist from the Central Bureau for Nuclear Measurements, Geel, Belgium.

Applied Physics Division
Argonne National Laboratory
9700 South Cass Avenue
Argonne, Illinois 60439
U.S.A.

NUCLEAR DATA AND MEASUREMENTS SERIES

The Nuclear Data and Measurements Series presents results of studies in the field of microscopic nuclear data. The primary objective is the dissemination of information in the comprehensive form required for nuclear technology applications. This Series is devoted to: a) measured microscopic nuclear parameters, b) experimental techniques and facilities employed in measurements, c) the analysis, correlation and interpretation of nuclear data, and d) the evaluation of nuclear data. Contributions to this Series are reviewed to assure technical competence and, unless otherwise stated, the contents can be formally referenced. This Series does not supplant formal journal publication but it does provide the more extensive information required for technological applications (e.g., tabulated numerical data) in a timely manner.

OTHER ISSUES IN THE ANL/NDM SERIES ARE:

ANL/NDM-1 Cobalt Fast Neutron Cross Sections-Measurement and Evaluation by P. T. Guenther, P. A. Moldauer, A. B. Smith, D. L. Smith and J. F. Whalen, July 1973.

ANL/NDM-2 Prompt Air-Scattering Corrections for a Fast-Neutron Fission Detector: $E_n \leq 5$ MeV by Donald L. Smith, September 1973.

ANL/NDM-3 Neutron Scattering from Titanium; Compound and Direct Effects by E. Barnard, J. deVilliers, P. Moldauer, D. Reitmann, A. Smith and J. Whalen, October 1973.

ANL/NDM-4 ^{90}Zr and ^{92}Zr; Neutron Total and Scattering Cross Sections by P. Guenther, A. Smith and J. Whalen, July 1974.

ANL/NDM-5 Delayed Neutron Data - Review and Evaluation by Samson A. Cox, April 1974.

ANL/NDM-6 Evaluated Neutronic Cross Section File for Niobium by R. Howerton, Lawrence Livermore Laboratory and A. Smith, P. Guenther and J. Whalen, Argonne National Laboratory, May 1974.

ANL/NDM-7 Neutron Total and Scattering Cross Sections of Some Even Isotopes of Molybdenum and the Optical Model by A. B. Smith, P. T. Guenther and J. F. Whalen, June 1974.

ANL/NDM-8 Fast Neutron Capture and Activation Cross Sections of Niobium Isotopes by W. P. Poenitz, May 1974.

ANL/NDM-9 Method of Neutron Activation Cross Section Measurement for E_n = 5.5-10 MeV Using the D(d,n)He-3 Reaction as a Neutron Source by D. L. Smith and J. W. Meadows, August 1974.

ANL/NDM-10 Cross Sections for (n,p) Reactions on ^{27}Al, $^{46,47,48}Ti$, $^{54,56}Fe$, ^{58}Ni, ^{59}Co and ^{64}Zn from Near Threshold to 10 MeV by Donald L. Smith and James W. Meadows, January 1975.

ANL/NDM-11 Measured and Evaluated Fast Neutron Cross Sections of Elemental Nickel by P. Guenther, A. Smith, D. Smith and J. Whalen, Argonne National Laboratory and R. Howerton, Lawrence Livermore Laboratory, July 1975.

ANL/NDM-12 A Spectrometer for the Investigation of Gamma Radiation Produced by Neutron-Induced Reactions by Donald L. Smith, April 1975.

ANL/NDM-13 Response of Several Threshold Reactions in Reference Fission Neutron Fields by Donald L. Smith and James W. Meadows, June 1975.

ANL/NDM-14 Cross Sections for the $^{66}Zn(n,p)^{66}Cu$, $^{113}In(n,n')^{113m}In$ and $^{115}In(n,n')^{115m}In$ Reactions from Near Threshold to 10 MeV by Donald L. Smith and James W. Meadows, July 1975.

ANL/NDM-15 Radiative Capture of Fast Neutrons in ^{165}Ho and ^{181}Ta by W. P. Poenitz, June 1975.

ANL/NDM-16 Fast Neutron Excitation of the Ground-State Rotational Band of ^{238}U by P. Guenther, D. Havel and A. Smith, September 1975.

ANL/NDM-17 Sample-Size Effects in Fast-Neutron Gamma-Ray Production Measurements: Solid-Cylinder Samples by Donald L. Smith, September 1975.

ANL/NDM-18 The Delayed Neutron Yield of ^{238}U and ^{241}Pu by J. W. Meadows January 1976.

ANL/NDM-19 A Remark on the Prompt-Fission-Neutron Spectrum of ^{252}Cf by P. Guenther, D. Havel, R. Sjoblom and A. Smith, March 1976.

ANL/NDM-20 Fast-Neutron-Gamma-Ray Production from Elemental Iron: $E_n \lesssim$ 2 MeV by Donald L. Smith, May 1976.

ANL/NDM-21 Note on the Experimental Determination of the Relative Fast-Neutron Sensitivity of a Hydrogenous Scintillator by A. Smith, P. Guenther and R. Sjoblom, June 1976.

ANL/NDM-22 Note on Neutron Scattering and the Optical Model Near A=208 by P. Guenther, D. Havel and A. Smith, September 1976.

ANL/NDM-23 Remarks Concerning the Accurate Measurement of Differential Cross Sections for Threshold Reactions Used in Fast-Neutron Dosimetry for Fission Reactors by Donald L. Smith, December 1976.

ANL/NDM-24 Fast Neutron Cross Sections of Vanadium and an Evaluated Neutronic File by P. Guenther, D. Havel, R. Howerton, F. Mann, D. Smith, A. Smith and J. Whalen, May 1977.

ANL/NDM-25 Determination of the Energy Scale for Neutron Cross Section Measurements Employing a Monoenergetic Accelerator by J. W. Meadows, January 1977.

ANL/NDM-26 Evaluation of the IN-115(N,N')IN-115M Reaction for the ENDF/B-V Dosimetry File by Donald L. Smith, December 1976.

ANL/NDM-27 Evaluated (n,p) Cross Sections of ^{46}Ti, ^{47}Ti and ^{48}Ti by C. Philis and O. Bersillon, Bruyeres-le-Chatel, France and D. Smith and A. Smith, Argonne National Laboratory, January 1977.

ANL/NDM-28 Titanium-II: An Evaluated Nuclear Data File by C. Philis, Centre d'Etudes de Bruyères-le-Châtel, R. Howerton, Lawrence Livermore Laboratory and A. B. Smith, Argonne National Laboratory, June 1977.

ANL/NDM-29 Note on the 250 keV Resonance in the Total Neutron Cross Section of ^{6}Li by A. B. Smith, P. Guenther, D. Havel and J. F. Whalen, June 1977.

ANL/NDM-30 Analysis of the Sensitivity of Spectrum-Average Cross Sections to Individual Characteristics of Differential Excitation Functions by Donald L. Smith, March 1977.

ANL/NDM-31 Titanium-I: Fast Neutron Cross Section Measurements by P. Guenther, D. Havel, A. Smith and J. Whalen, May 1977.

ANL/NDM-32 Evaluated Fast Neutron Cross Section of Uranium-238 by W. Poenitz, E. Pennington, and A. B. Smith, Argonne National Laboratory and R. Howerton, Lawrence Livermore Laboratory, October 1977.

ANL/NDM-33 Comments on the Energy-Averaged Total Neutron Cross Sections of Structural Materials by A. B. Smith and J. F. Whalen, June 1977.

ANL/NDM-34 Graphical Representation of Neutron Differential Cross Section Data for Reactor Dosimetry Applications by Donald L. Smith, June 1977.

ANL/NDM-35 Evaluated Nuclear Data File of Th-232 by J. Meadows, W. Poenitz, A. Smith, D. Smith and J. Whalen, Argonne National Laboratory and R. Howerton, Lawrence Livermore Laboratory, February 1978.

ANL/NDM-36 Absolute Measurements of the $^{233}U(n,f)$ Cross Section Between 0.13 and 8.0 MeV by W. P. Poenitz, April 1978.

ANL/NDM-37 Neutron Inelastic Scattering Studies for Lead-204 by D. L. Smith and J. W. Meadows, December 1977.

ANL/NDM-38 The Alpha and Spontaneous Fission Half-Lives of ^{242}Pu by J. W. Meadows, December 1977.

ANL/NDM-39 The Fission Cross Section of ^{239}Pu Relative to ^{235}U from 0.1 to 10 MeV by J. W. Meadows, March 1978.

ANL/NDM-40 Statistical Theory of Ne itron Nuclear Reactions by P. A. Moldauer, February 1978.

ANL/NDM-41 Energy-Averaged Neutron Cross Sections of Fast-Reactor Structural Materials by A. Smith, R. McKnight and D. Smith, February 1978.

ANL/NDM-42 Fast Neutron Radiative Capture Cross Section of ^{232}Th by W. P. Poenitz and D. L. Smith, March 1978.

ANL/NDM-43 Neutron Scattering from ^{12}C in the Few-MeV Region by A. Smith, R. Holt and J. Whalen, September 1978.

ANL/NDM-44 The Interaction of Fast Neutrons with ^{60}Ni by A. Smith, P. Guenther, D. Smith and J. Whalen, January 1979.

ANL/NDM-45 Evaluation of $^{235}U(n,f)$ between 100 KeV and 20 MeV by W. P. Poenitz, July 1979.

ANL/NDM-46 Fast-Neutron Total and Scattering Cross Sections of ^{107}Ag in the MeV Region by A. Smith, P. Guenther, G. Winkler and J. Whalen, January 1979.

ANL/NDM-47 Scattering of MeV Neutrons from Elemental Iron by A. Smith and P. Guenther, March 1979.

ANL/NDM-48 ^{235}U Fission Mass and Counting Comparison and Standardization by W. P. Poenitz, J. W. Meadows and R. J. Armani, May 1979.

ANL/NDM-49 Some Comments on Resolution and the Analysis and Interpretation of Experimental Results from Differential Neutron Measurements by Donald L. Smith, November 1979.

ANL/NDM-50 Prompt-Fission-Neutron Spectra of ^{233}U, ^{235}U, ^{239}Pu and ^{240}Pu Relative to that of ^{252}Cf by A. Smith, P. Guenther, G. Winkler and R. McKnight, September 1979.

ANL/NDM-51 Measured and Evaluated Neutron Cross Sections of Elemental Bismuth by A. Smith, P. Guenther, D. Smith and J. Whalen, April 1980.

ANL/NDM-52 Neutron Total and Scattering Cross Sections of ^{6}Li in the Few MeV Region by P. Guenther, A. Smith and J. Whalen, February 1980.

ANL/NDM-53 Neutron Source Investigations in Support of the Cross Section at the Argonne Fast-Neutron Generator by James W. Meadows and Donald L. Smith, May 1980.

ANL/NDM-54 The Nonelastic-Scattering Cross Sections of Elemental Nickel by A. B. Smith, P. T. Guenther and J. F. Whalen, June 1980.

ANL/NDM-55 Thermal Neutron Calibration of a Tritium Extraction Facility using the $^{6}Li(n,t)^{4}He/^{197}Au(n,\gamma)^{198}Au$ Cross Section Ratio for Standardization by M. M. Bretscher and D. L. Smith, August 1980.

ANL/NDM-56 Fast-Neutron Interactions with ^{182}W, ^{184}W and ^{186}W by P. T. Guenther, A. B. Smith and J. F. Whalen, December 1980.

ANL/NDM-57 The Total, Elastic- and Inelastic-Scattering Fast-Neutron Cross Sections of Natural Chromium, Peter T. Guenther, Alan B. Smith and James F. Whalen, January 1981.

ANL/NDM-58 Review of Measurement Techniques for the Neutron Capture Process by W. P. Poenitz, August 1981.

ANL/NDM-59 Review of the Importance of the Neutron Capture Process in Fission Reactors, Wolfgang P. Poenitz, (to be published).

ANL/NDM-60 Neutron Capture Activation Cross Sections of ^{94}, ^{96}Zr, $^{98,100}Mo$, and $^{110,114,116}Cd$ at Thermal and 30 keV Energy, John M. Wyrick and Wolfgang P. Poenitz, (to be published).

ANL/NDM-61 Fast-neutron Total and Scattering Cross Sections of ^{58}Ni by Carl Budtz-Jørgensen, Peter T. Guenther, Alan B. Smith and James F. Whalen, September 1981.

ANL/NDM-62 Covariance Matrices and Applications to the Field of Nuclear Data, by Donald L. Smith, Nobember 1981.

ANL/NDM-63 On the Neutron Inelastic-scattering Cross Sections of ^{232}Th, ^{233}U, ^{235}U, ^{238}U, ^{239}Pu, and ^{240}Pu, Alan B. Smith and Peter T. Guenther, (to be published).

TABLE OF CONTENTS

THE FISSION FRAGMENT ANGULAR DISTRIBUTIONS AND TOTAL KINETIC ENERGIES FOR $^{235}U(n,f)$ FROM .18 to 8.83 MeV[a]

by

J. W. Meadows and Carl Budtz-Jørgensen[b]

Applied Physics Division
Argonne National Laboratory
9700 South Cass Avenue
Argonne, Illinois 60439

ABSTRACT

A gridded ion chamber was used to measure the fission fragment angular distribution and total kinetic energy for the $^{235}U(n,f)$ reaction from 0.18 to 8.81 MeV neutron energy. The anisotropies are in generally good agreement with earlier measurements. The average total kinetic energy is ~ 0.2 MeV greater than the thermal value at neutron energies < 2 MeV and shows a sudden decrease of ~ 0.8 MeV between 4 and 5 MeV neutron energy, well below the (n, n'f) threshold. Possible causes of this decrease are a change in the mass distribution or decreased shell effects in the heavy fragment.

[a]This work supported by the U.S. Department of Energy.

[b]Visiting scientist from the Central Bureau for Nuclear Measurements, Geel, Belgium.

I. INTRODUCTION

It has long been known that the signal induced in a parallel plate ion chamber by the formation of an ion pair is dependent on position.[1] Recently, Knitter and Budtz-Jørgensen[2] developed a detector system and data processing procedure which exploits this property and permits the measurement of the angular distribution, as well as the total energy, of fission fragments using a gridded ion chamber. A similar system has been assembled at the Argonne National Laboratory Fast Neutron Generator (FNG) facility and used to measure the fragment angular distribution and average kinetic energy of the $^{235}U(n,f)$ reaction from thermal energies to ~ 9 MeV. One of the reasons for making this series of measurements was to gain experience in using this equipment. ^{235}U was ideal for this purpose. Samples were readily available, the large thermal neutron fission cross section provided a convenient reference point, and the fast neutron fission cross section was large enough to obtain good statistical accuracy in reasonable times. Furthermore, the fragment angular distribution had been fairly well determined by previous measurements using several techniques. Leachman and Blumberg[3] and Simmons and Henkel[4] have covered this energy range, while several investigators [5-10] have reported results at lower energies with generally good agreement.

Less is known concerning the dependence of the average fragment kinetic energy on neutron energy although several measurements have been reported.[11-16] A measurement by Blyumkina et al.[11] indicated a sudden increase at ~ 0.4 MeV neutron energy and also showed a similar increase for ^{233}U near 0.2 MeV. The ^{233}U results were confirmed by subsequent measurements,[12] but the ^{235}U results were not. The only measurements at substantially higher energies were made by D'yachenko et al.[16] who made measurements up to 7 MeV, with an isolated point at 15 MeV. They observed little change in the kinetic energy below 3.5 MeV, but their results do indicate a substantial decline somewhere between 3.5 and 5 MeV.

This report describes the operation of the detector system and presents the results of the angular distribution and average kinetic energy measurements for the $^{235}U(n,f)$ reaction from thermal to 8.8 MeV neutron energy.

II. EXPERIMENTAL APPARATUS

Protons or deuterons were accelerated in the FNG to produce neutrons by the $^{7}Li(p,n)^{7}Be$ and $D(d,n)^{3}He$ reactions. Neutrons with energies < 5 MeV were produced using targets formed by evaporating thin layers of lithium metal onto tantalum target cups. Neutrons with energies > 5 MeV were produced by deuterons incident onto a thin window gas target[17] filled with deuterium gas. Low energy neutrons from the secondary source reactions such as $^{7}Li(p,n)^{7}Be^{*}$, $^{7}Li(p,^{3}H\ n)^{4}He$ and D(d,np)D were present for some primary neutron energies and corrections were calculated using the information on their relative intensity and energy spectra given in refs. 18 and 19. The background produced by (d,n) reactions in the gas target structure was measured by bombarding the empty gas target at each energy. Very low energy neutrons from room scattering were responsible for 3-4% of the total fissions at all energies. The FNG energy was controlled by a 90 deg. analyzing magnet and slit feedback system that was calibrated by observing the thresholds for the $^{7}Li(p,n)^{7}Be$, $^{11}B(p,n)^{11}C$ and $^{27}Al(p,n)^{27}Si$ reactions.[20-21]

The detector was a double-gridded ion chamber with a common cathode, mounted so the chamber axis coincided with the FNG beam line. The ^{235}U deposits were mounted on both sides of the cathode. These were prepared by molecular deposition[22] of highly enriched (99.86%) ^{235}U. The chamber was constructed of stainless steel with polytetrafluoroethylene insulators. It was operated as a flow chamber, and a constant absolute pressure was maintained by means of a pressure regulator of the cartesian diver type. The chamber design and dimensions were chosen with the following requirements in mind: (1) Fission fragments must stop within the volume defined by the cathode and grid. (2) The grid must effectively shield the anode from ions in the active volume. (3) The electrode structure should be rigid. (4) The detector structure should be as light as practical to minimize neutron scattering. The experimental set-up is shown in Fig. 1. The essential chamber dimensions and operating conditions are listed in Table I.

Each fission produced a cathode and an anode signal in one of the detectors. The pairs of cathode and anode pulses were digitized to 1024 channels each, tagged to indicate the detector of origin, and sent to an on-line computer system which stored them sequentially on a magnetic disk and provided running displays for monitoring equipment operation. All processing was done off-line.

III. EXPERIMENTAL METHOD

The basic theory of ion chamber operation is discussed in Ref. 1 and the method for obtaining angular distribution information is covered by Knitter and Budtz-Jørgensen.[2] A summary and the essential results are given below.

Consider a fast-parallel-plate ion chamber with a grid inserted between the anode and cathode at a distance d from the cathode. It is assumed that electron capture is negligible and that the amplifier time constants are long compared to the electron transit time, but very short compared to the positive ion transit time. An electron-positive-ion pair is formed at distance y from the cathode. After amplification the cathode signal is

$$P_c = g_c \left(1 - \frac{y}{d}\right) \qquad (1)$$

where g_c is a constant that is proportional to the amplifier gain. If several ion pairs are formed, the total signal is the superposition of the signals produced by the individual ion-pairs. If they are formed along the track of a fission fragment originating at the cathode, the cathode signal is

$$P_c = g_c \int_0^{R(E)} \left(1 - X\frac{\cos\theta}{d}\right)\rho(E,X)\,dX \qquad (2)$$

where θ is the angle of the track with respect to the normal to the electrodes, X is the distance along the track, E is the initial energy of the fragment, $\rho(E,X)$ is the ionization density, and R(E) is the fragment range.

Both ρ and R are dependent on the mass and charge of the fragment as well as its energy. Only the dependence on energy is considered in the following discussion since fission fragments of a given energy are usually confined to a small range of mass and charge. The second term in eq. (2) can be defined as

$$N\bar{X}(E) = \int_0^{R(E)} X\rho(E,X)dX \qquad (3)$$

where N is the number of ion pairs formed. If the ionization defect of ~5 MeV is ignored, N may be regarded as being proportional to the initial fragment energy, E, and eq. (2) can be written as

$$P_c = G_c\, E\left(1 - \frac{\bar{X}(E)}{d}\cos\theta\right) \qquad (4)$$

No signal appears at the anode until the electrons began to pass through the grid. Since they all appear to originate at the same distance from the anode and since the induction effects of the positive ions are eliminated by the grid, the magnitude of the anode signal is

$$P_a = G_a E \qquad (5)$$

where G_a is dependent on the gain in the anode amplifier and contains other factors that are also common to G_c. The ratio of the two signals is

$$P_{c/a}(\cos\theta,E) = \frac{G_c}{G_a}\left(1 - \frac{\bar{X}(E)}{d}\cos\theta\right) \qquad (6)$$

This depends only on the angle of the track and two constants: a proportionality constant, G_c/G_a, which is the ratio of the amplifier gains and $\bar{X}(E)/d$ which depends on the energy of the fragment. For calculational purposes, $\bar{X}(E)/d$ is redefined as

$$\bar{X}(E)/d = P_{c/a}(0,E) - P_{c/a}(1,E) \qquad (7)$$

then

$$\cos\theta = \frac{P_{c/a}(\cos\theta E) - P_{c/a}(0,E)}{\bar{X}(E)d} \qquad (8)$$

The value of $\cos\theta$ associated with any fragment is readily determined if $P_{c/a}(0,E)$ and $P_{c/a}(1,E)$ are known. For $\cos\theta = 0$, all the ion pairs appear to originate at the cathode and the same charge signal will appear at both the cathode and the anode. This is implied by eq. (6) which also shows that $P_{c/a}(0,E)$ will be independent of E. In real detectors, few fragments with $\cos\theta = 0$ are seen since they do not normally leave the deposit. However, identical charge signals can be forced on the anode and cathode by temporarily converting the detector into a non-gridded ion chamber. The anode and grid are connected together, the cathode is biased at $V_c - V_g$ and the anode electronics are connected to the anode-grid combination. Since charge sensitive preamplifiers are used, any change in capicitance has negligible effect on the signal.

In order to locate $P_{c/a}(1,E)$, a fission spectrum was collected to good statistical accuracy ($> 10^5$ fissions) and converted to a two-parameter array with the anode signal as one channel and $P_{c/a}$ as the other. For each energy channel, there is a distribution of $P_{c/a}$ extending from a channel corresponding $\cos\theta = 0$ to one corresponding to $\cos\theta = 1$. This is illustrated in Fig. 2 for ~ 5 MeV energy intervals located near the low and high energy peaks. $\bar{X}(E)/d$ was determined according to eq. (7) for a number of energies and converted into an interpolation table for use in calculating $\cos\theta$.

The distributions illustrated in Fig. 2 were derived from thermal neutron induced fission of ^{235}U and ideally should be flat. However, there is a pronounced drop for channels corresponding to $\cos\theta > 0.35$. This is a consequence of choosing energy intervals at or slightly above the positions of the fission peaks. Energy losses in the deposits result in a net loss of events in these intervals. On the low energy side of the peaks, energy channels show a net gain for small values of $\cos\theta$.

The above discussion assumes that the anode is completely shielded from the induction of the positive ions and that no electrons are collected by the grid. Actually, a fraction (σ) of the lines of force pass through the grid and end on the anode and a fraction (λ) of the electrons are collected by the grid. The cathode signal is not affected but the anode signal becomes

$$P_a = G_a E(1 - \lambda)\left[1 - \sigma \frac{\bar{X}}{d} \cos\theta\right] \quad . \tag{9}$$

λ is not a constant but depends on location. σ is a constant but its effect is position dependent. Since these effects cause a spread in the anode signal with a corresponding increase in the angular and energy resolution of the chamber, it is best to construct the chamber so as to make them as small as practical

The dependence of λ and σ on chamber dimensions is discussed in Ref. 1. For small σ and small $2\pi a/s$

$$\sigma \sim \frac{s}{2\pi b} \ln \frac{s}{2\pi a} \tag{10}$$

where s is the grid wire spacing, b is the grid-anode distance and a is the grid wire radius. In the present chamber $\sigma \sim .018$. Since $\bar{X}/d \lesssim 0.5$, the effect on P_a is < 1%. An actual estimate of λ is the more difficult but complete electron collection is achieved when

$$\frac{V_a - V_g}{V_g - V_c} \frac{d}{a} \gtrsim \frac{S + 2\pi a}{S - 2\pi a} \tag{11}$$

where V_a, V_g, and V_c are the anode, grid, and cathode voltages, respectively. In the present chamber that condition is exceeded by 50%.

IV. THE ANGULAR DISTRIBUTION MEASUREMENT

Once $P_{c/a}(0,E)$ and a table of $\bar{X}(E)/d$ vs. E have been determined, values of cosθ can be assigned to each fragment observed. Fig. 3a illustrates the cosθ distribution for thermal fission in the forward detector. The shape is nearly rectangular as expected for an isotropic distribution. The effect of the ~ 5% cos θ resolution[2] can be seen at cos θ = 1. There is some loss of events near cos θ = 0 due to the finite sample thickness. Measurements made with other samples show that this is definitely a sample thickness effect and not an instrumental one. The loss is much greater for thicker samples but distributions obtained with a self-transferred ^{252}Cf source were flat over the full range of cos θ. Fig. 3b shows the cos θ distribution for the same detector at 7.6 MeV. In order to correct for distortions induced by the uranium deposit and by the angular resolution, the final angular distribution was obtained by dividing the 7.6 MeV results by the thermal distribution. The results, corrected for the center of mass motion, are shown in Fig. 4. The curve is the results of a least squares fit, and

$$W(\theta)/W(90) = 1.362 \pm 0.026 \cos^2\theta.$$

Normally, explicit corrections for the center of mass motion were not made. Instead, the distributions from the forward and backward detectors were averaged. This effectively corrected for the center of mass motion as long as the center of mass momentum was much less than the fragment momentum.

All the angular distributions were fitted with a polynominal of the type

$$W(\theta) = \sum_{K=0}^{n} a_k \cos^{2K}\theta \tag{12}$$

The best fit (based on a chi squared test) for about two-thirds of the measurements was obtained with n = 1. In most of the remaining cases

higher order polynominals gave only slight improvement so all anisotropies were based on n = 1 fits. Corrections were made for lower energy neutrons from room scattering and from the secondary source reactions (Section II). The anisotropies, defined as

$$\frac{W(0)}{W(90)} - 1 \tag{13}$$

are listed in Table II and are plotted in Fig. 5 where they are compared with several other measurements.[3-5,9,10] The agreement is fairly good at all energies. The increase in the anisotropy beginning at ~ 6 MeV is very well correlated with the increase in fission cross section[23] due to second chance fission. The negative anisotropy at low neutron energies observed by Hsue et al.[9] and Ahmad et al.[10] is confirmed.

V. THE AVERAGE KINETIC ENERGY

The kinetic energy measurements were based on the anode signal which was proportional to N, the number of ion pairs formed in the detector. Schmitt and Leachman[24] have demonstrated that for a fragment of energy E,

$$E = \omega N + \Delta, \tag{14}$$

where ω is the energy loss per ion pair and Δ is the ionization defect. Although ω shows a weak dependence on fragment mass, it is not sensitive to the energy. However, the ionization defect is mass dependent. Still, any change in the average fragment energy will be reflected in N as long as there is no drastic change in the mass distribution.

Energy loss in the uranium deposits made the average anode signal dependent on the fragment angle and consequently on the angular distribution. The effect was eliminated by dividing the cosθ-fragment-energy distribution into 8 equal intervals in cosθ. Then, the average kinetic energy, $\bar{E}$, relative to the value for thermal neutron induced fission, $\bar{E}(E_{th})$, is

$$\bar{E}(E_n) = \bar{E}(E_{th}) \left[\sum_i^k \bar{P}_j \, (E_n) \Big/ \sum_i^k \bar{P}_j \, (E_{th}) \right] \tag{15}$$

where E_n is the incident neutron energy, i and k specify the range of cosθ intervals, and $\bar{P}_j$ is the average pulse height for the j^{th} interval. The thermal fission value for $\bar{E}(E_{th})$ was assumed to be 170 MeV. Only intervals 5-8 (0-60 deg.) were used to calculate $\bar{E}$ since the energy spectra in the first intervals were badly distorted due to energy loss in the deposits and to fragment scattering. Averaging the results for the forward and backward detectors effectively corrected for the center of mass motion. Corrections for fissions induced by lower energy neutrons from secondary source reactions and room scattering were made by an interation procedure. These corrections were generally small; less than 0.01 MeV at most energies. However, at the highest energy point for their respective targets, the correction for the D(d,np)D reaction was -0.26 MeV and the correction for the ^{7}Li(p,^{3}H n)^{4}He reaction was -0.15 MeV.

The correction for neutron emission from the fragments was

$$\Delta E_n(E_n) = \frac{1}{2}\left(\frac{\bar{E}_L}{\bar{M}_L} + \frac{\bar{E}_H}{\bar{M}_H}\right)\left[\left(\bar{\nu}_p(E_n) - \frac{\sigma_{II}(E_n)}{\sigma_F(E_n)}\right) - \bar{\nu}_p(E_{th})\right] \qquad (16)$$

where E_L and E_H are the average energies of the light and heavy fragments, M_L and M_H are their average masses, ν_p is the average number of prompt neutrons emitted, σ_F is the total fission cross section and σ_{II} is the second chance fission cross section. Values of $\bar{\nu}_p$ and σ_F were taken from Ref. 23. It was assumed that all neutrons were emitted isotropically from the fully accelerated fragments and that equal numbers were emitted by the light and heavy fragments. The first chance fission cross section above the second chance threshold was estimated by extending the σ_F curve with a line tangent to it at 5.3 MeV and reaching 1.0 b at 10 MeV.

The consistency of the energy measurements was tested by determining the effect of the incident neutron momentum on the average fragment energy and comparing it with the expected values. $\Delta\bar{E}_m$ is defined as the change in the average fragment energy produced by the incident neutron momentum. The expected value, relative to $\bar{E}(E_{th})$, is

$$\Delta\bar{E}_m = 2\left(\frac{M_n \bar{M}_L \bar{M}_H}{M^3\, \bar{E}(E_{th})}\right)^{1/2} (\cos\theta_k + \cos\theta_i)\, E_n^{1/2} \qquad (17)$$

where M_n is the neutron mass, M is the mass of the compound nucleus, and $\theta_i - \theta_k$ is the range of angles covered in the measurement. $\Delta\bar{E}_m$ is the same in both directions except for sign. Experimentally,

$$(\Delta E_m)_{exp} = \frac{\bar{E}_F(E_n,\theta_i,\theta_k) - \bar{E}_B(E_n,\theta_i,\theta_k)}{2\bar{E}(E_{th},\theta_i,\theta_k)} \quad . \qquad (18)$$

Corrections must be made for the lower energy neutrons from the secondary source reactions and from room scattering, but no correction for neutron emission is necessary since this should be the same in both directions. The results for the 0-60 deg. interval are plotted in Fig. 6 and compared with the expected values. The agreement is good.

The results of the average kinetic energy measurements are reported in Table II and compared with other measurements[11,15,16] in Figs. 7 and 8 where

$$\Delta\bar{E}(E_n) = \bar{E}(E_{th}) - \bar{E}(E_n) \quad . \qquad (19)$$

At the lower neutron energies $\Delta\bar{E}$ is generally positive. An average

of the data below 2 MeV gives 0.22 ± 0.06 MeV. There is a slow decline to ~ 4 MeV then a precipitous decrease of ~ 0.8 MeV between 4 and 5 MeV. Above 5 MeV, $\Delta\overline{E}$ is constant with an average value of -0.80 ± 0.06 MeV. There is no significant effect in the region of the (n,n'f) threshold. Blyumkina et al.[11] have reported a step of ~ 0.7 MeV near 0.4 MeV neutron energy with a corresponding change in the number of prompt neutrons. These data show no such step and measurements by Ajitanand and Boldeman[15] find $\Delta\overline{E} \approx 0$ from 0.2 to 0.9 MeV. D'yachenko et al.[13,14,16] have reported a number of measurements. They find $\Delta\overline{E}$ to be ~ +0.2 MeV below 2 MeV neutron energy and ~ -0.4 MeV above 5 MeV.

Present ideas about the fission process place severe restrictions on any change in the total kinetic energy. The total fission energy, E_T, is the sum of the energy brought in by the incident particle and the energy derived from the division of the compound nucleus. The following relation[25] holds along the fission path between the saddle and scission points for a single fission channel:

$$E_T = E_p + E_k + E^* \tag{20}$$

where E_p is the potential energy, E_k is the pre-scission kinetic energy and E^* is the excitation energy. At scission, the total kinetic energy is

$$E = E_k^s + E_c \tag{21}$$

where E_c is the coulomb repulsion energy at scission. The excitation energy of the fragments is

$$E_f^* = E^{*s} + E_d^s \tag{22}$$

where E_d^s is the deformation energy at scission. If the collective and internal degrees of freedom are strongly coupled, any change in E_p is shared among all degrees of freedom and E_k^s is small. If the coupling is weak, E_p is converted into E_k. Fission through other channels may produce different values of E for the same mass division. With strong coupling, this can happen only if a modification in the configuration at scission produces a change in E_c. With weak coupling, there may be a change in both E_k^s and E_c. These changes are not large, but if only a few fission channels are available, then the opening of a single additional channel may produce an observable change in E.

The degree of coupling is an open question and the kinetic energy for symmetric fission as a function of $Z^2/A^{1/3}$ has been explained equally well by both strong and weak coupling.[26,27] Boldeman et al.[12] have assumed weak coupling and calculated the energy dependence of $\Delta\overline{E}$ for ^{233}U and ^{235}U from 0.01 to 0.6 MeV by channel analyses of the fission cross section using a double-humped fission barrier and similar transition state spectra. They implicitly assumed that the mass division and E_c was the same for all channels. Then

$$\overline{E}_p(E_n) = \sum_\alpha \sigma_\alpha(E_n) E_{p\alpha} \Big/ \sum_\alpha \sigma_\alpha(E_n) \tag{23}$$

and

$$\Delta\overline{E}(E_n) = \overline{E}_p(E_n) - \overline{E}(0) \tag{24}$$

where α is the fission channel and σ_α is the channel cross section. However, they found $\Delta\bar{E} \approx 0$ for ^{235}U.

This result was a consequence of the transition state spectrum used. Since the fission barrier for these nuclei lies just below the excitation energy corresponding to E_n=0, the nucleus is cold as it passes the barrier, and for E_n less than a few hundred keV there is not enough energy available to split a nucleon pair in even-even nuclei. Thus, the properties of the fission channels are determined by a sequence of collective vibrational levels and their associated rotational bands. The lowest energy levels have positive parity.[28] Since the ^{235}U ground state has negative parity, thermal fission must proceed through the higher energy negative parity channels. With increasing neutron energy, p-wave neutrons become available and fission can proceed through the lower energy positive parity channels as well as higher energy channels of both parities and the resulting values of $\Delta\bar{E}$ are nearly zero. The ^{233}U ground state has positive parity so thermal fission can proceed through the lowest levels. With increasing neutron energy higher energy states become available with a corresponding increase in $\Delta\bar{E}$. These results are in fairly good agreement with the experimental data[11,28] on ^{233}U and with their own measurements[15] on ^{235}U, but are not in agreement with D'yachenko et al.[13,14,16] or with the present work. The data presented in this report shows a definite bias toward positive values at low neutron energies. An average of all points below 1 MeV gives +0.18 ± 0.08 MeV.

The most prominent feature of the present work is the sudden decrease of $\bar{E}$ by ~ 0.8 MeV near 4.5 MeV neutron energy. At this energy the number of fission channels is large and the opening of a few additional ones should have little effect. However, changes in the mass distribution or in the deformation at the scission point could easily affect $\bar{E}$ by this amount.

Krick and Evans[29] have observed that the delayed neutron yield for $^{235}U(n,f)$ decreases rapidly between 4 and 5 MeV although it shows no significant change below that energy. This indicates a change in the delayed neutron precursor yields and suggests that there is a significant change in the mass-charge distribution of the fragments. The total kinetic energy is a function of the fragment mass ratio, being low for both symmetric and very asymmetric fission, so a broader mass distribution and an increase in the symmetric fission yield can cause a decrease in $\bar{E}$. A rudimentary calculation shows how $\bar{E}$ is affected by reasonable changes in these factors. The gross features of the heavy fragment mass distribution can be represented by

$$Y(M_H) = \left[Y_a(M_H - 139) + AY_s(M_H - 118) \right] \Big/ (1 + A) \qquad M_H \geq 118 \tag{25}$$

where Y_a and Y_s are normalized Gaussians with widths determined by their variance, σ^2, a and s refer to the symmetric and antisymmetric components, and A is chosen to give the observed peak-to-valley ratio. Glendenin et al[30] have found that the peak-to-valley ratio for $^{235}U(n,f)$ decreases exponentially with increasing E_n up to the (n,n'f) threshold. It is approximately given by

$$p/v \approx 500\exp(-0.55\ E_n) \quad . \tag{26}$$

For the asymmetric mass peaks σ^2 increases significantly[31] from thermal to 6 MeV neutron energy although the energy dependence is uncertain. It is given an exponential dependence on the assumption that the cause of the increase is related to the increased symmetric yield.

$$\sigma^2 \approx 30 + \exp(0.45E_n) \quad . \tag{27}$$

The mass dependent kinetic energy, taken as the thermal data in Ref. 31 and assumed to be independent of E_n, was averaged over the distribution of Eq. (25). The results are compared with the experimental data in Fig. 9. In a qualitative sense the agreement is surprisingly good. The calculated $\Delta\bar{E}$ is near the observed value at 6 MeV although the precipitous decline near 4.5 MeV is not reproduced.

Wilkins et al.[32] have described a more fundamental process that may be responsible for the decrease in $\bar{E}$. A decrease in shell effects with increasing excitation energy results in a more elongated configuration at the scission point. Since the charge centers are further apart there is a decrease in coulomb repulsion and a corresponding decrease in $\bar{E}$. They have reproduced the general trend of the mass and charge distributions and total kinetic energy using a static scission-point model where the total potential energy at scission is the sum of the liquid-drop energies of the nascent fragments with shell and pairing correction terms plus coulomb and nuclear interaction terms. With no shell and pairing terms a potential minimum exists, for all mass divisions, with large deformations for each fragment. When the correction terms are added the potential minima for asymmetric mass divisions of ^{236}U are usually displaced toward less total deformation. With increasing excitation energy the shell effects decrease and the minima move back toward the liquid-drop values. The total deformation increases and there is a drop in the total kinetic energy. Normally, this is a gradual process but for some mass divisions the deformation can change quite rapidly. For the 134/102 mass division at low excitation energies there is a large shell correction and the location of the deepest potential minimum corresponds to a nearly spherical heavy fragment. The total deformation is ~ 30% less than the liquid-drop value. However, there is a secondary minimum near the position of the liquid-drop minimum that is produced by a combination of shell and liquid-drop terms. As the shell corrections decrease this becomes the deeper minimum at some point and when this occurs there is a rapid increase in its relative contribution to the fission yield. Since the deformation is much larger for the second minimum there is a decrease in the kinetic energy.

Some experimental evidence bearing on this analysis may be obtained from Ref. 31. A comparison of the total kinetic energy data for thermal and 6 MeV neutron energy shows that $E(6) - E(E_{th}) \geq 2$ MeV for $126 < M_H < 136$ and < 1 MeV for other mass values. These are provisional mass values and no correction has been made for neutron emission but these corrections make no qualitative difference. There is a well defined range of mass divisions where the change in kinetic energy is unusually large.

For a given mass division any decrease in E must result in an increase in E_f^* with a corresponding in the number of fission neutrons, ν. If other factors are held constant this will also be true for the average over the mass distribution. Soleilhac et al.[33] have reported $\bar{\nu}_p$ measurements in this energy region with data points at about 1 MeV intervals but they find no effect. They do find a small step near 6 MeV but that is well above the 4-5 MeV region and appears to be related to the onset of the (n,n'f) reaction.

However, $\bar{\nu}_p$ does depend on several factors and a change in $\bar{E}$ does not necessarily affect it. The mass dependence of E_T is similar to the mass dependence of E except that the minimum for symmetric fission is not so pronounced. A broader mass distribution will give a decrease in $\bar{E}_T$ as well as in $\bar{E}$ and the increase in E_f^* is substantially reduced. If decreasing shell effects are responsible for the step in the $\bar{E}$ shown in Fig. 8 then relative neutron separation energies become important. Examination of the potential surface plot for the 134/102 mass division in Ref. 32 shows that a transfer to the second minimum causes a decrease in the deformation of the light fragment and an increase in the deformation of the heavy fragment. There will be corresponding changes in the fragment excitation energies and if the neutron separation energies for the light fragment are low relative to those of the heavy fragment then any effect on $\bar{\nu}_p$ will be reduced.

Table I. Ion Chamber Dimensions and Operating Conditions

Electrode Diameter	12.0 cm
Grid Diameter	8.9 cm
Grid Wire Diameter	0.1 mm
Grid Wire Spacing	1.0 mm
Grid-Cathode Distance	3.2 cm
Grid-Anode Distance	1.0 cm
Uranium Deposits	
Diameter	2.5 cm
Thickness (0 deg. Detector)	76 μg U/cm^2
Thickness (180 deg. Detector)	54 μg U/cm^2
Counter Gas	90% Ar
	10% CH_4
Operating Pressure	810 millitorr
Cathode Voltage	-2900 Volts
Grid Voltage	-1400 Volts
Anode Voltage	0 Volts
Amplifier Time Constants	3 μsec

Table II. The Fission Fragment Anisotropies and Average Kinetic Energies

E_n (MeV)	E_n[a] (MeV)	W(0)/W(90) -1	Error[b]	$\bar{E}$ (MeV)	Error[b] (MeV)
0.179	0.024	-0.03	0.015	0.269	0.200
0.298	0.024	0.017	0.016	0.073	0.200
0.467	0.022	0.067	0.016	-0.053	0.200
0.598	0.021	0.093	0.016	0.357	0.199
0.748	0.020	0.079	0.016	0.326	0.200
0.896	0.020	0.119	0.016	0.134	0.197
1.046	0.020	0.097	0.016	0.484	0.197
1.108	0.020	0.147	0.016	0.128	0.200
1.459	0.034	0.163	0.012	0.267	0.143
1.992	0.030	0.214	0.012	0.201	0.141
2.491	0.028	0.201	0.013	0.042	0.146
2.990	0.026	0.159	0.016	0.039	0.178
3.254	0.047	0.168	0.020	0.026	0.219
3.490	0.024	0.160	0.016	0.160	0.178
3.760	0.044	0.153	0.020	-0.034	0.221
3.964	0.024	0.178	0.016	0.017	0.178
4.274	0.041	0.155	0.020	-0.020	0.221
4.514	0.040	0.174	0.020	-0.432	0.221
5.19	0.14	0.153	0.025	-0.850	0.292
5.48	0.13	0.174	0.023	-0.469	0.264
5.76	0.11	0.155	0.022	-0.644	0.256
6.04	0.10	0.168	0.021	-1.045	0.240
6.31	0.09	0.243	0.020	-0.575	0.241
6.58	0.08	0.374	0.035	-0.833	0.256
6.84	0.08	0.376	0.032	-1.012	0.245
7.10	0.08	0.364	0.031	-0.663	0.231
7.36	0.08	0.296	0.024	-1.363	0.228
7.61	0.08	0.395	0.028	-0.756	0.216
7.86	0.07	0.335	0.027	-0.925	0.218
8.12	0.07	0.379	0.027	-0.515	0.207
8.36	0.07	0.353	0.028	-0.930	0.204
8.58	0.07	0.401	0.028	-0.695	0.202
8.83	0.07	0.380	0.027	-0.707	0.192

[a]Resolution. Full width at half maximum.

[b]Statistical error.

REFERENCES

1. D. H. Wilkinson, "Ionization Chambers and Counters," University Press, Cambridge (1950).

2. H. H. Knitter and Carl Budtz-Jørgensen, "New Fission Fragment Detectors for Cross Section and Angular Distribution Measurements at CBNM," Proc. Int. Conf. Nuclear Cross Sections for Technology, Knoxville, Tenn., October 22-26, 1979, NBS Special Publication 594, U.S. National Bureau of Standards (1980).

3. R. B. Leachman and L. Blumberg, Phys. Rev., 137B 814(1965).

4. J. E. Simmons and R. L. Henkel, Phys. Rev., 120 198(1960).

5. V. G. Nesterov, G. N. Smirenkin and D. L. Shpak, Sov. J. Nucl. Phys., 4 173(1967).

6. D. M. Nadkarni, S. S. Kapoor and P. N. Rama Rao, "Angular Distribution of Fission Fragments in the Neutron Induces Fission of U-235 near Threshold," Proceedings of a Symposium on Nuclear Physics and Solid State Physics, Vol. II, p. 133, Bombay (1968).

7. R. L. Walsh, J. W. Boldeman, J. Carnana and J. N. Mathur, "Odd-Even Effects in the Total Energy Release in Fission and Angular Distribution of Fission Fragments," Proceedings of a Symposium on Nuclear Physics and Solid State Physics, Vol. 2, p. 92, Bombay (1974).

8. G. N. Smirenkin, D. L. Shpak, Yu. B. Ostapenko, and B. I. Furson, JETP Lett., 11 333(1970).

9. S. T. Hsue, G. F. Knoll and J. W. Meadows, Nucl. Sci. Eng., 66 24(1978).

10. S. Ahmad, M. M. Islam, A. H. Khan, M. Khaliquazzaman, M. Husain, and M. A. Rahman, Nucl. Sci. Eng., 71 208(1979).

11. Yu. A. Blyumkina, I. I. Bondarenko, V. F. Kuznetsov, V. G. Nesterov, V. N. Okolovitch, G. N. Smirenkin, and L. N. Vsachev, Nucl. Phys., 52 648(1964).

12. J. W. Boldeman, W. K. Bertram and R. L. Walsh, Nucl. Phys., A265 337(1976).

13. P. P. D'yachenko, B. D. Kuz'menov and M. Z. Tarasko, Sov. J. Nucl. Phys., 8 165(1968).

14. P. P. D'yachenko, B. D. Kuz'menov and A. Lajatai, Phys. Letters, 31B 122(1970).

15. N. N. Ajitanand and J. W. Boldeman, Nucl. Phys., A144 1(1970).

16. P. P. D'yachenko, B. D. Kuz'menov, L. S. Kutsaeva, and V. M. Piksaikin, Sov. J. Nucl. Phys., 14 629 (1972).

17. J. W. Meadows, D. L. Smith and G. Winkler, Nucl. Instr. and Meth., 176 439(1980).

18. J. W. Meadows and D. L. Smith, "Neutrons from Proton Bombardment of Natural Lithium," ANL-7938, Argonne National Laboratory (1972).

19. D. L. Smith and J. W. Meadows, "A Method of Neutron Activation Cross Section Measurement Using the $D(d,n)^3He$ Reaction as a Neutron Source," ANL/NDM-9, Argonne National Laboraotry (1974).

20. J. B. Marion, Rev. Mod. Phys., 38 660(1966).

21. E. H. Beckner, R. L. Bramblett and G. C. Phillips, Phys. Rev., 123 2100(1961).

22. W. Parker, H. Bilkstein and N. Getoff, Nucl. Instr. and Meth., 26 55(1964).

23. ENDF/B Summary Documentation, BNL-NCS-17451 (ENDF-201), 3rd ed. (ENDF/B-V), R. Kinsey, Ed., available from the National Nuclear Data Center, Brookhaven National Laboratory (July 1979).

24. H. W. Schmitt and R. B. Leachman, Phys. Rev., 102 183(1956).

25. A. Michaudon, "Neutrons and Fission," Proceeding International Conference on the Interactions of Neutrons with Nuclei, Lowell, Mass., July 6-9, 1976.

26. K. T. R. Davies, A. J. Sierk and J. R. Nix, Phys. Rev. C, 13C 2385(1976).

27. J. Blocki, Y. Boneh, J. R. Nix, J. Randrup, M. Robel, A. J. Sierk, and J. W. Swiatecki, Ann. Phys., 113(1978).

28. B. B. Back, J. P. Bondrof, G. A. Otrochenko, J. Pedersen, and B. Rasmussen, Nucl. Phys., A165 449(1971).

29. M. S. Krick and A. E. Evans, Nucl. Sci. Eng., 47 311(1972).

30. L. E. Glendenin, J. E. Gindler, D. J. Henderson, and J. W. Meadows, Phys. Rev., 24C 2600(1981).

31. J. W. Meadows, Phys. Rev., 177 1817(1968).

32. B. D. Wilkins, E. P. Steinberg and R. R. Chasman, Phys. Rev. C, 14, 1832 (1976).

33. M. Soleilhac, J. Frehaut and J. Gauriau, J. of Nucl. Energy, 23 257(1969).

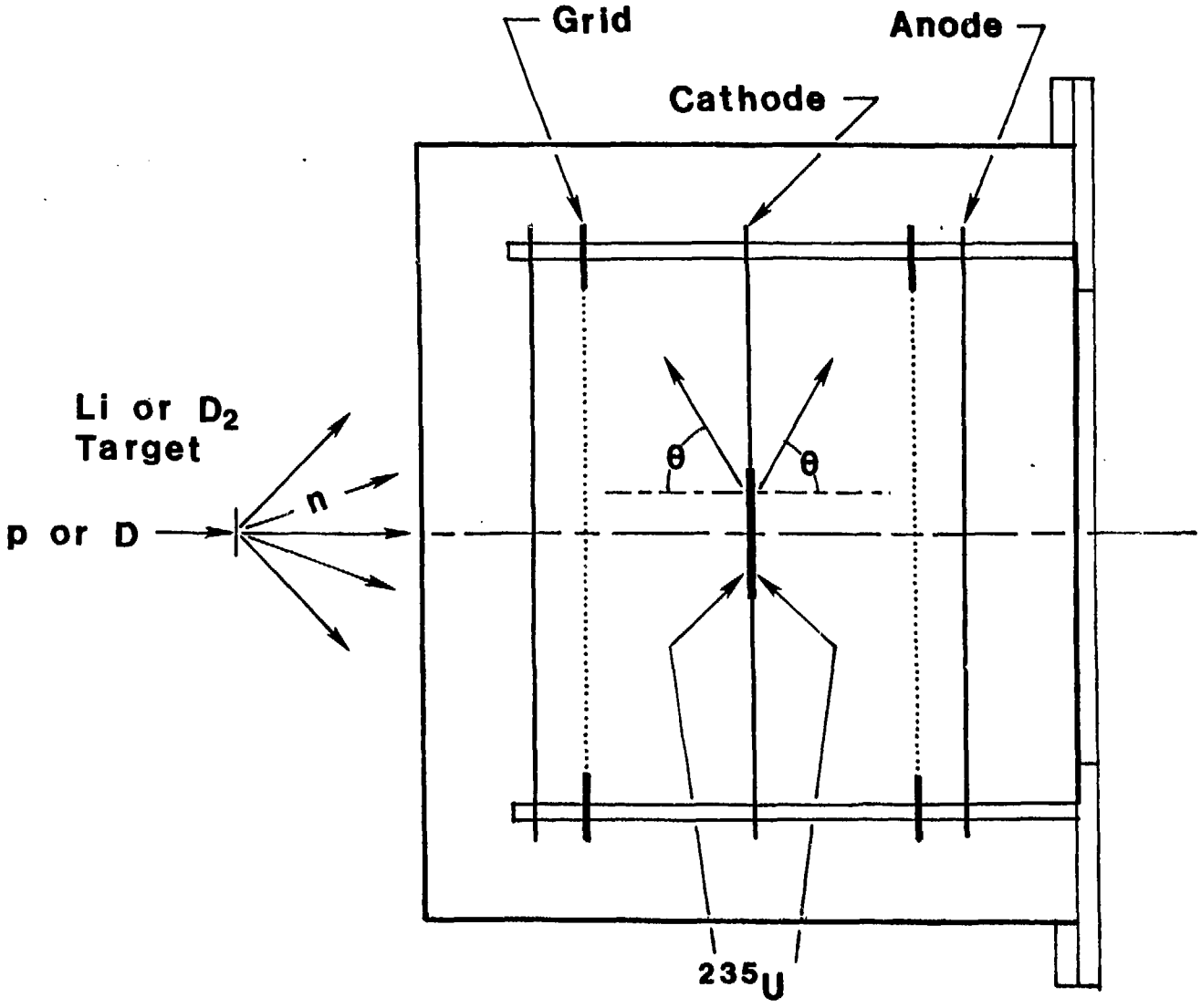

Fig. 1. A schematic diagram of the experimental arrangement.

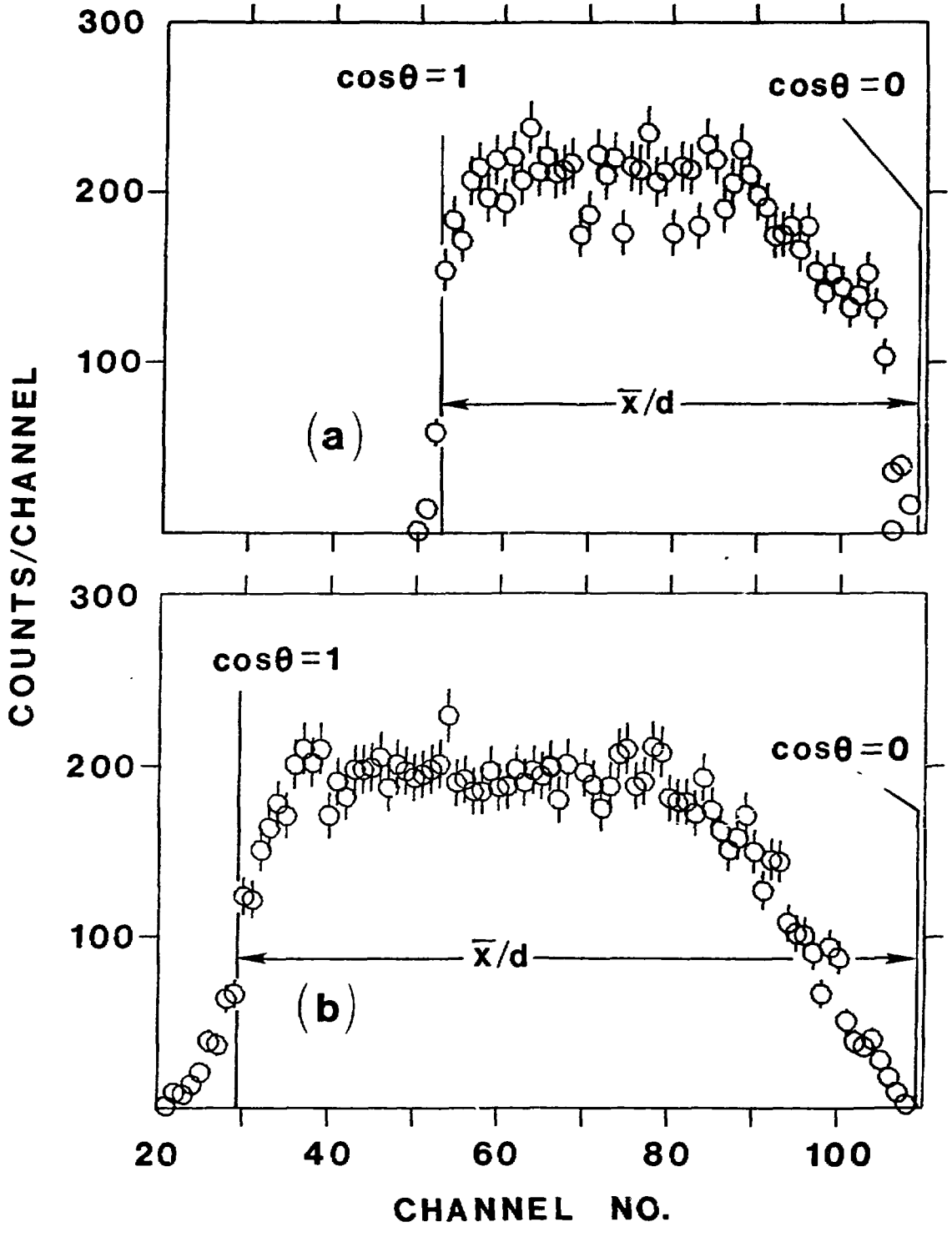

Fig. 2. The distribution of P_c/P_a for 5 MeV energy intervals: (a) low energy peak, (b) high energy peak.

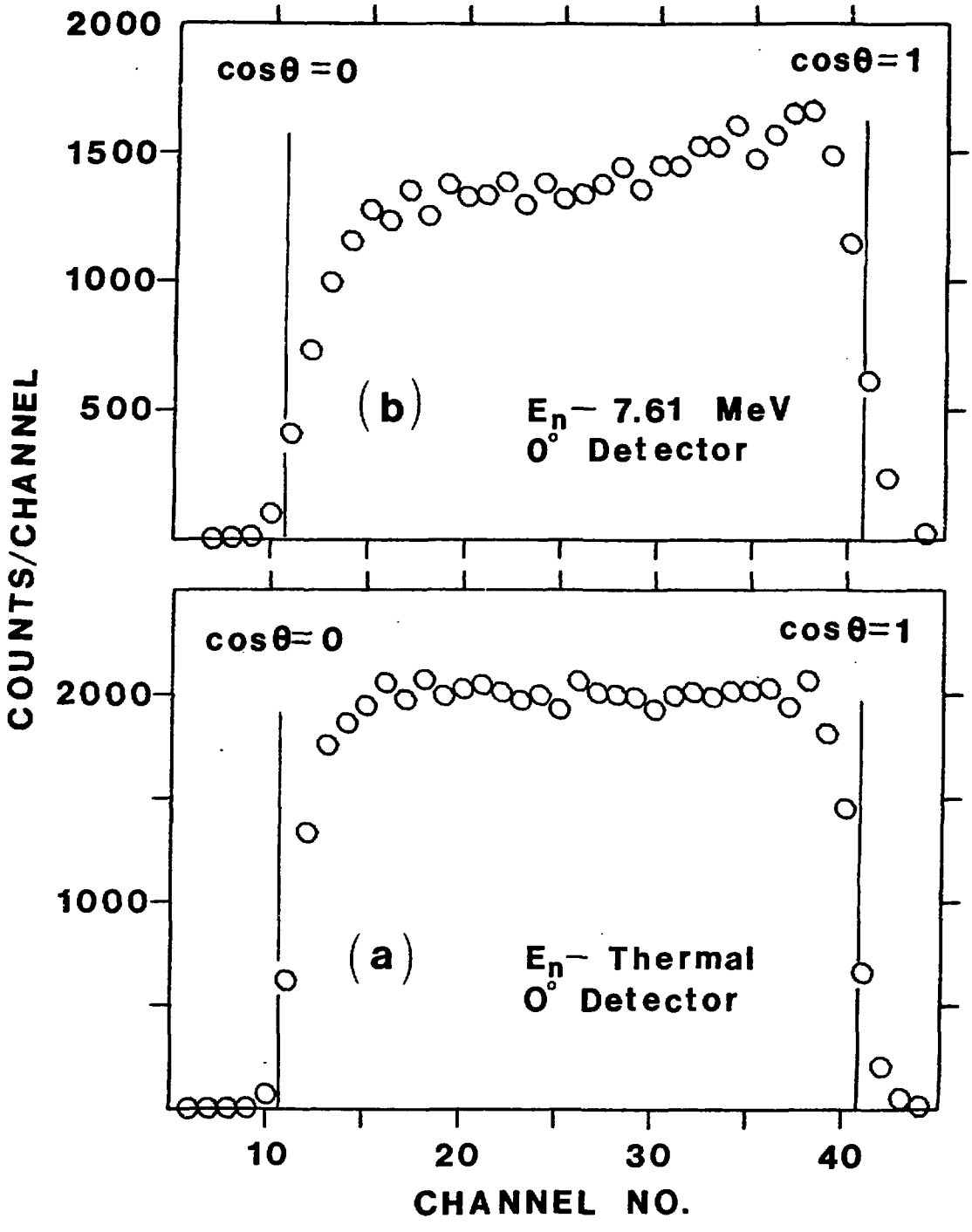

Fig. 3. The distribution of cosθ as calculated from the experimental data for the forward detector. The distributions were calculated using eq. (8).

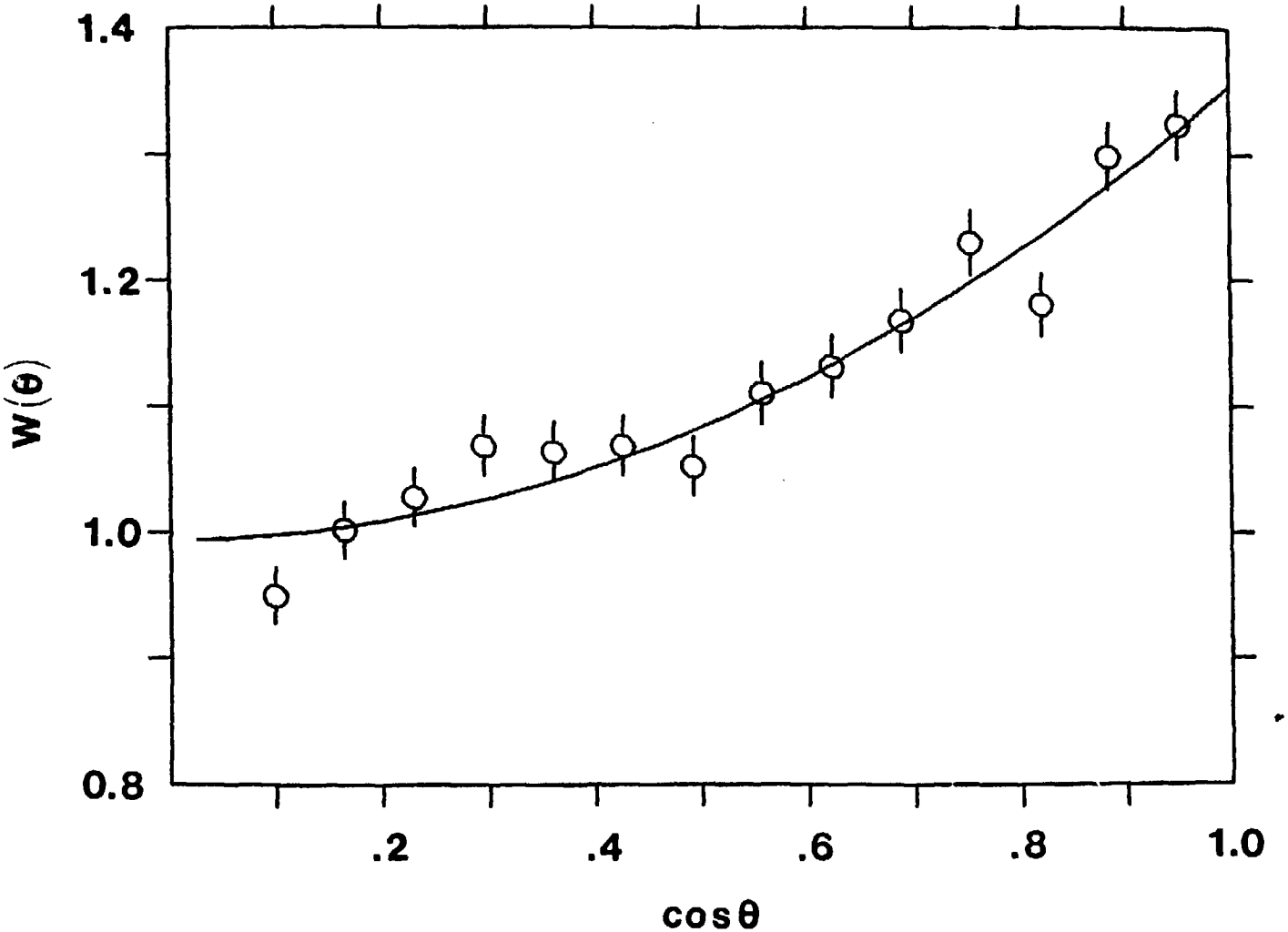

Fig. 4. The angular distribution at 7.61 MeV obtained from the data in Fig. 2. The results have been corrected for center-of-mass motion.

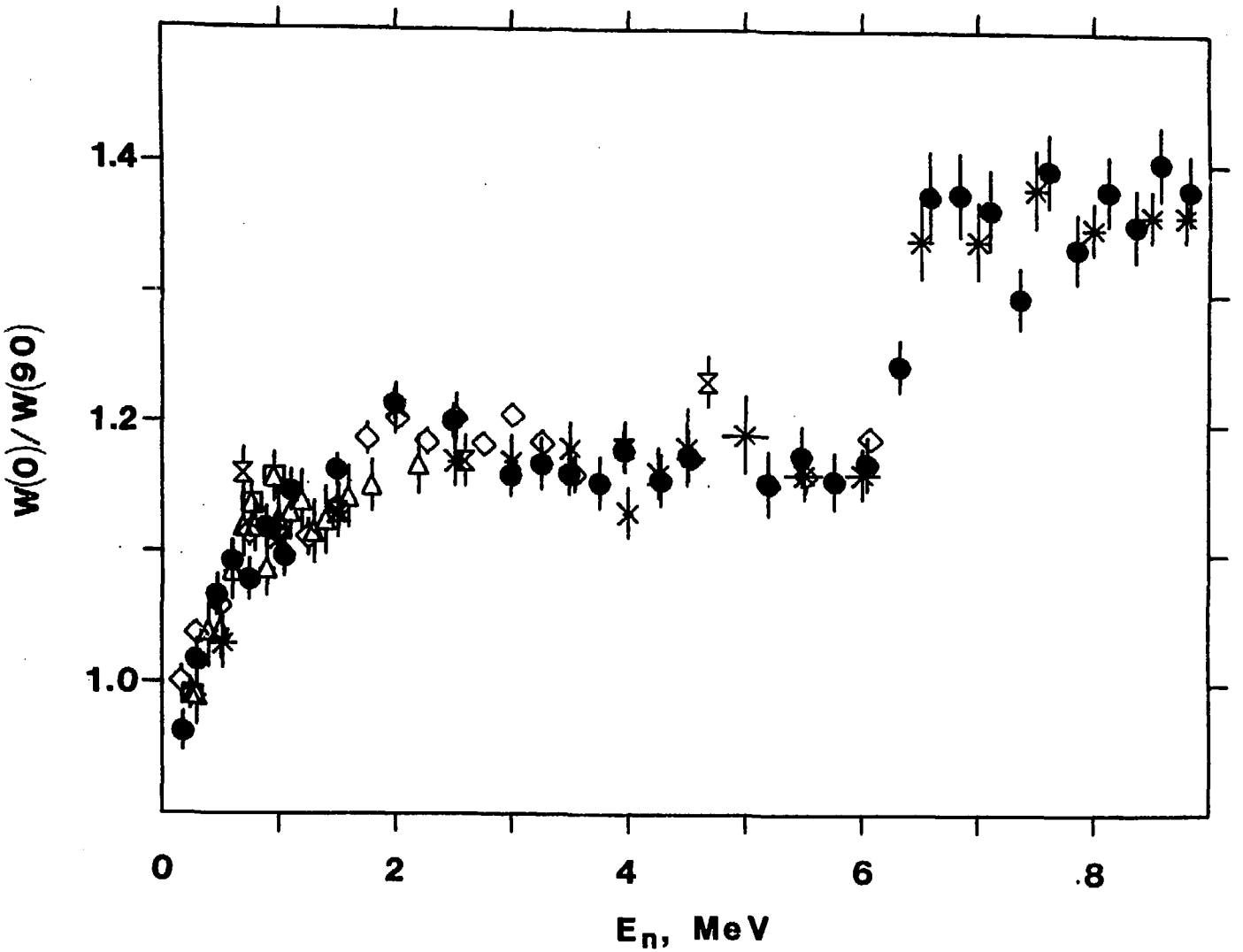

Fig. 5. W(0)/W(90) versus neutron energy for $^{235}U(n,f)$. O - the present work, X - ref. 3, X - ref. 4, ◇ - ref. 5, ▣ - ref. 9, Δ - ref. 10.

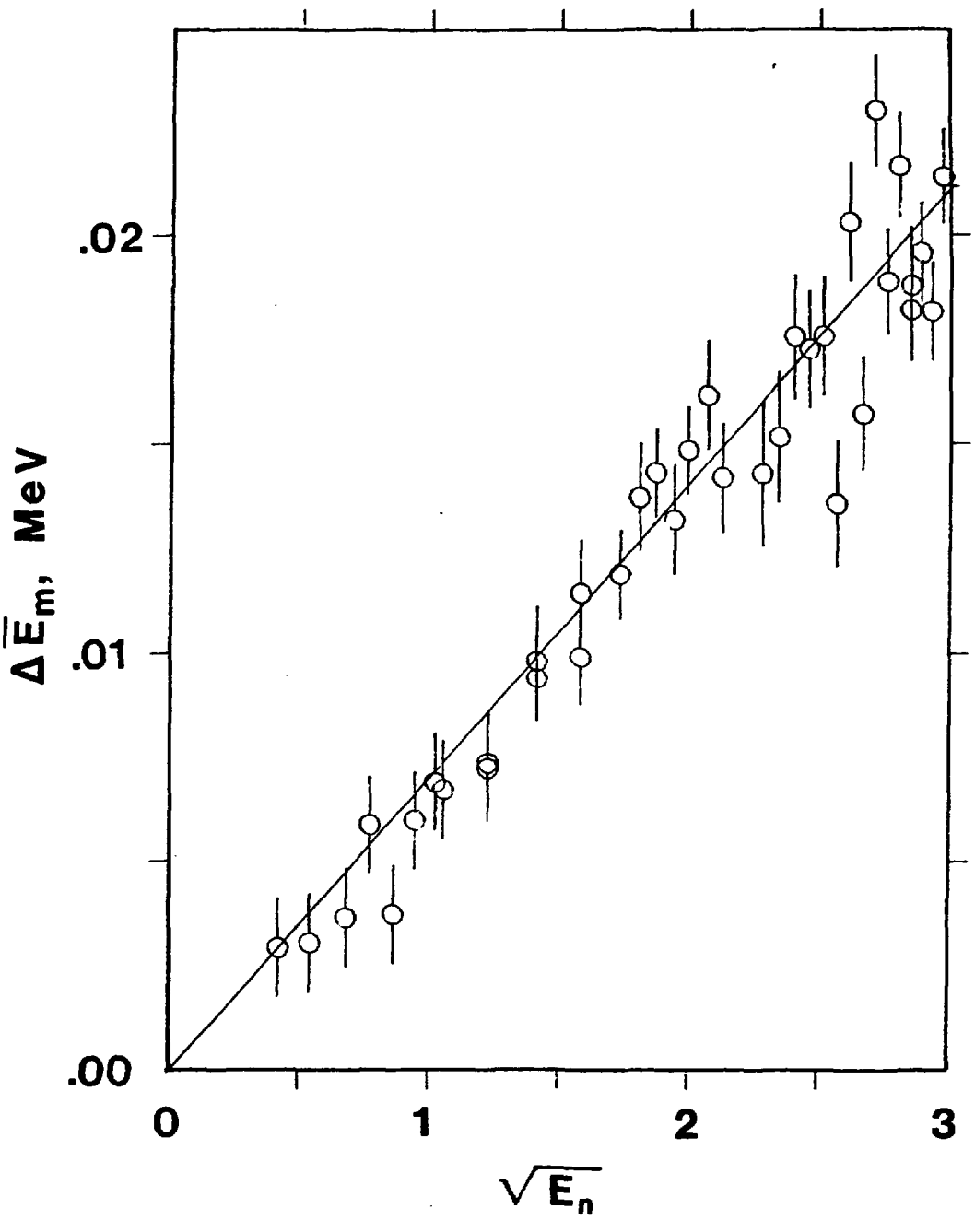

Fig. 6. The effect of the center-of-mass motion on the average total kinetic energy for a single detector compared with the expected values. The angular range is 0-60 deg. and the angular distribution effects have been removed.

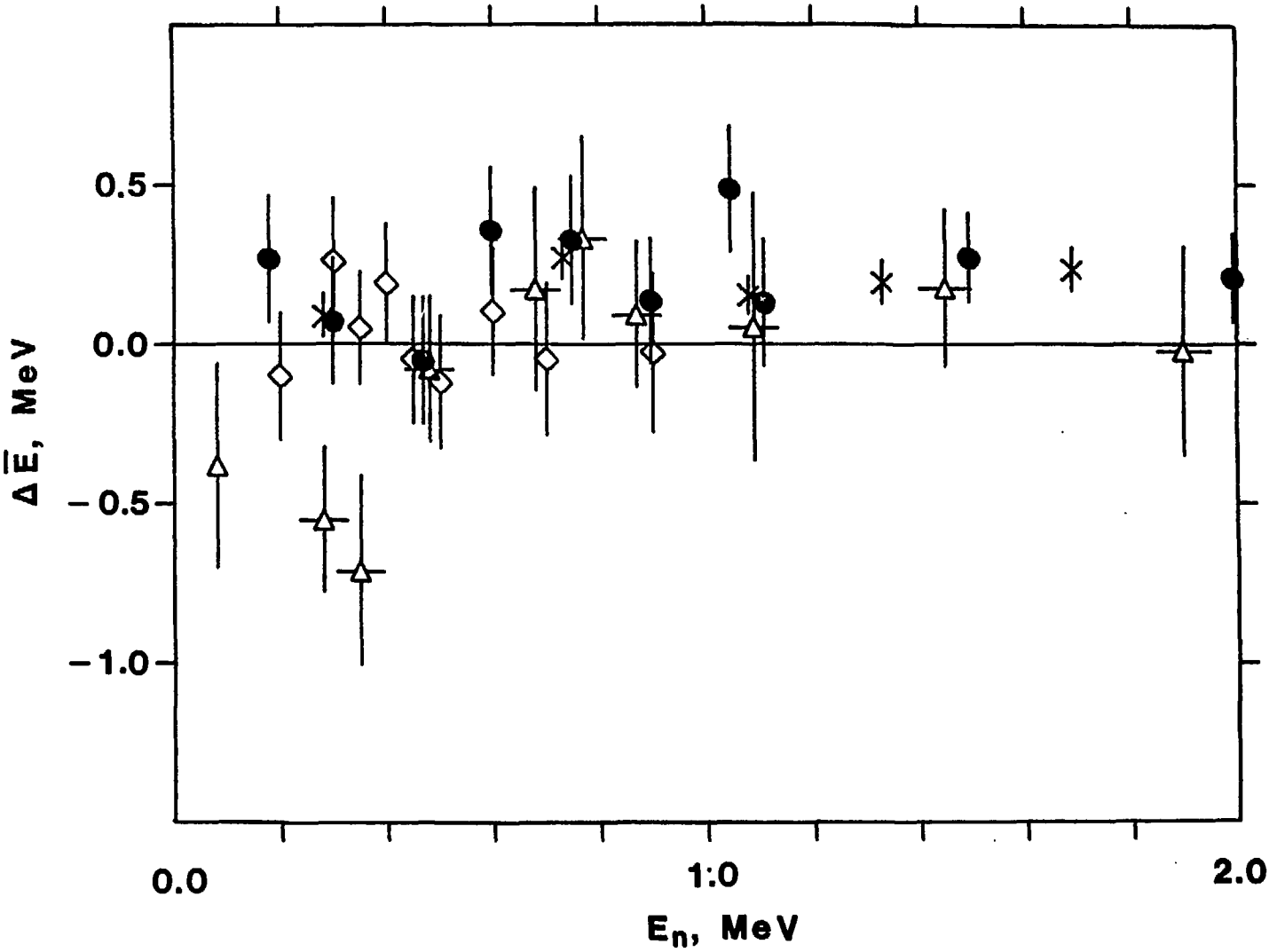

Fig. 7. The change in the average total kinetic energy relative to the thermal value for neutron energies 2 MeV. O - the present work, Δ - ref. 11, ◇ - ref. 15, X - ref. 16.

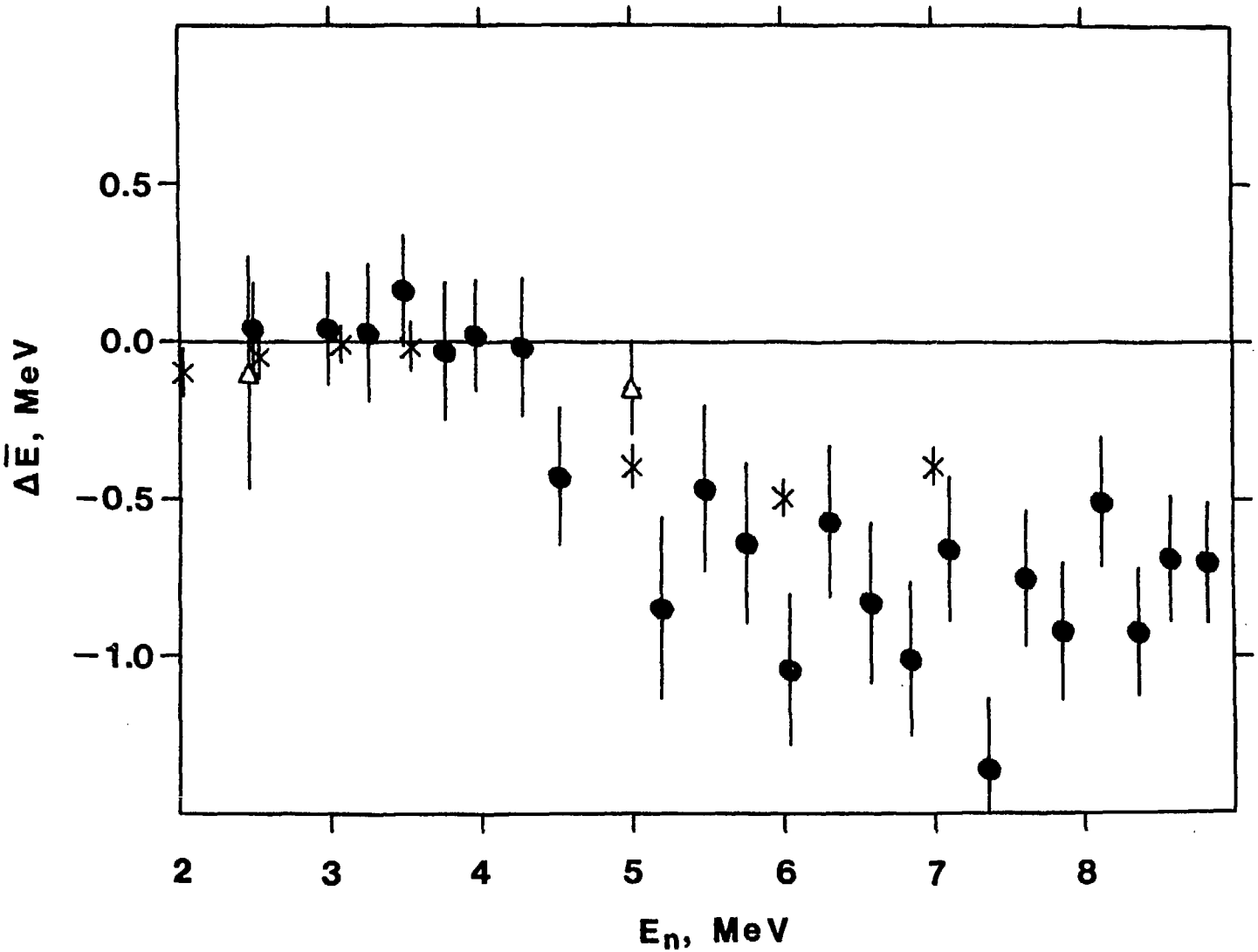

Fig. 8. The change in the average total kinetic energy relative to the thermal value for neutron energies 2 MeV. O - the present work, Δ - ref. 11, X - ref. 16.

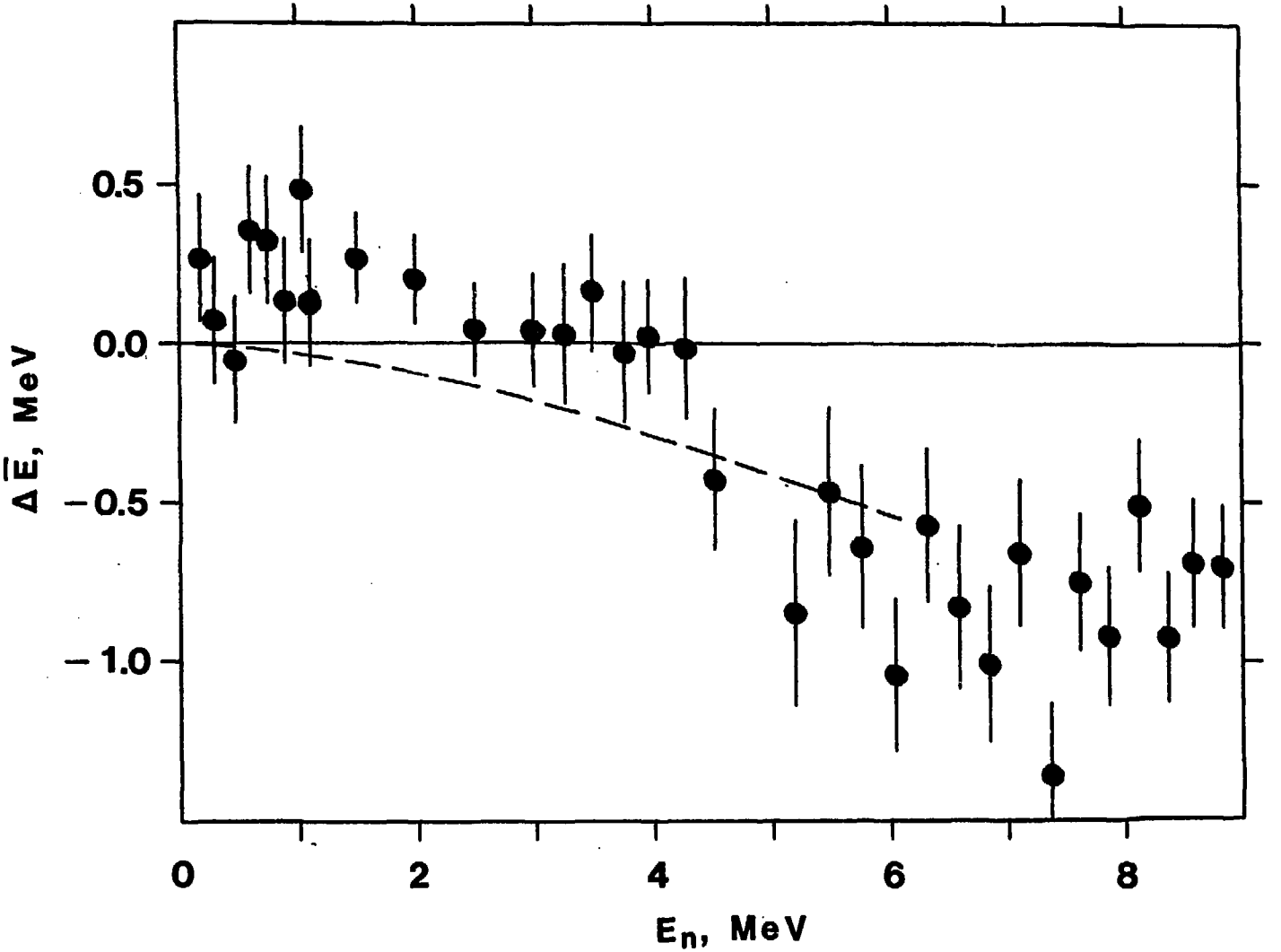

Fig. 9. The change in the average total kinetic energy relative to the thermal value compared with the values calculated from the change in the mass distribution.